Characterisation of dielectric 3D-printing materials at microwave frequencies

Andrea Alimenti[1], Kostiantyn Torokhtii[1], Nicola Pompeo[1], Emanuele Piuzzi[2], Enrico Silva[1]

[1] *Dipartimento di Ingegneria, Università degli Studi Roma Tre, 00146 Roma, Italy*
[2] *Dipartimento di Ingegneria dell'Informazione, Elettronica e Telecomunicazioni, Sapienza Università di Roma, Roma, Italy*

ABSTRACT
3D-printer materials are becoming increasingly appealing, especially for high frequency applications. As such, the electromagnetic characterisation of these materials is an important step in evaluating their applicability for new technological devices. We present a measurement method for complex permittivity evaluation based on a dielectric loaded resonator (DR). Comparing the quality factor *Q* of the DR with a disk-shaped sample placed on a DR base, with *Q* obtained when the sample is substituted with an air gap, allows a reliable determination of the loss tangent.

Corresponding author: Andrea Alimenti, e-mail: andrea.alimenti@uniroma3.it

1. INTRODUCTION

In recent years, the fast development and improvement of 3D-printing technologies has had a significant impact on many areas of human activity [1]-[5]. Printed materials are now utilised in high-frequency applications such as telecommunication technologies and microwave frequencies [6]-[12]. Thus, a reliable and handy electromagnetic (e.m.) characterisation of these materials is increasingly required [13].

In this work, the microwave characterisation of plastic 3D-printing materials is performed using a resonant perturbative technique. The physical quantity under investigation is permittivity ε, which is defined as the quantity (in a more general sense, the tensor) that describes the proportionality between the electric displacement vector $\boldsymbol{D}$ and the electric field strength vector $\boldsymbol{E}$ in a medium, $\boldsymbol{D} = \varepsilon_0 \boldsymbol{\varepsilon} \cdot \boldsymbol{E}$, with ε_0 being the vacuum permittivity. In the case of the materials studied here, after one accounts for the isotropic, homogeneous and linear limits, then $\varepsilon = \tilde{\varepsilon}$ is a scalar quantity that does not depend on positioning. The scalar complex relative permittivity is defined as $\tilde{\varepsilon} = \varepsilon' - i\varepsilon''$, where the real part ε' is a measure of the energy storage properties of the medium, while the imaginary part ε'' is related to the e.m. losses, and $i = \sqrt{-1}$. Since $\tilde{\varepsilon}$ is a complex quantity, it is often represented on the complex plane, where the angle δ

between $\tilde{\varepsilon}$ and the real axis is known as a loss angle. Thus, the ratio $\varepsilon''/\varepsilon' = \tan\delta$ is called the loss tangent.

In this work, a microwave ($\sim 12.9\,\mathrm{GHz}$) measurement method based on a resonant technique is proposed. The dielectric loaded resonator (DR) presented here was designed considering the e.m. properties of the dielectric materials usually used in 3D-printing and exploiting the possibility, given by 3D-printers, of shaping the samples in almost every desired shape. In the paper, an in-depth uncertainty analysis shows how the designed resonator is optimized to provide the best accuracy for this kind of material [14]. However, it is clear that its use is not limited only to 3D-printing plastics but to every kind of material electromagnetically and mechanically similar to them.

Moreover, to improve the repeatability of the measurement, the DR was specially designed to measure $\tilde{\varepsilon}$ by placing the dielectric sample on one of its flat bases, removing the need to disassemble and reassemble the whole structure for each measurement and thus reducing the uncertainties involved. DRs are well known for their high sensitivity [15] but also for poor measurement repeatability [16], [17], particularly in relation to resonant frequency. Thus, a closed structure is especially useful for characterising samples as it reduces the systematic errors inevitably introduced by each mounting procedure. Moreover, since it is not necessary to reassemble the resonator for each measurement, the measurement time is reduced.

A part of the volume of the resonating structure is substituted with the dielectric material under study. Comparison of the changes induced by the insertion of the sample on the unloaded quality factor Q and the resonant frequency f_0 can be used to evaluate the electric/magnetic properties of the sample. If the changes to the distribution of the e.m. field caused by the insertion of the sample are 'small', the resonant medium perturbation method [15] can be used.

Dielectric printed materials are already used for high frequency applications, and some works have explored their dielectric permittivity. Of particular note is the result obtained in [18], where acrylonitrile butadiene styrene (ABS) doped with different quantities of $BaTiO_3$ microparticles gave $2.6 < \varepsilon' < 8.7$ and $0.005 < \tan \delta < 0.027$, thus opening up the possibility of engineering these materials for specific uses. The measurements were performed at 15 GHz with a split post dielectric resonator obtaining $u(\tan \delta)/\tan \delta \sim 0.4\,\%$. The split post resonator is a very sensitive measurement instrument but does have some critical issues related to its assembly procedure [15]. The resonator presented in this work is tuned to a similar frequency (~ 12.9 GHz) and has a somewhat reduced sensitivity compared with the split post resonator but a much improved ease of operation – a useful feature in view of the routine measurements required.

In Sec. 2, the measurement method and system are presented. Then, in Sec. 3, a detailed uncertainties analysis is provided, while the results are shown in Sec. 4. Finally, conclusions are given in Sec. 5, comparing the obtained results to those given by a standard waveguide transmission/reflection method and to other relevant scientific works [13], [18], [19].

2. DESCRIPTION OF THE METHOD

A special configuration of a Hakki–Coleman dielectric loaded resonator [20] was designed to guarantee enhanced measurement repeatability at room temperature. The two physical quantities that characterise the response of the resonator are the unloaded quality factor Q and the resonant frequency f_0. Q is defined as $Q = \omega_0 W/P$, where W is the energy stored into the resonator at the resonant angular frequency $\omega_0 = 2\pi f_0$ and P is the power dissipated at the same frequency. Thus, as will be shown below, one can obtain information about the dielectric losses of the material under study (i.e. $\tan\delta$) from the Q measurement.

P is the sum of all the power losses $P = P_S + P_\Omega + P_V$, where the subscripts S, Ω, V indicate the quantities related, respectively, to the sample, to the metal surfaces and to all the other dielectric materials inside the resonator volume. Hence:

$$\frac{1}{Q} = \frac{P_S + P_\Omega + P_V}{\omega_0 W} = \frac{1}{Q_S} + \frac{1}{Q_\Omega} + \frac{1}{Q_V}, \tag{1}$$

with:

$$\frac{1}{Q_S} = \frac{\int_{V_S} \varepsilon_S'' \varepsilon_0 |\mathbf{E}|^2 dV}{2W} = \left[\frac{\varepsilon_S' \int_{V_S} \varepsilon_0 |\mathbf{E}|^2 dV}{2W} \right] \frac{\varepsilon_S''}{\varepsilon_S'} = \eta_S \tan\delta, \tag{2}$$

$$\frac{1}{Q_\Omega} = \sum_i \frac{\int_{S_i} R_i |\mathbf{H}_\tau|^2 dS}{2W} = \sum_i \frac{R_i}{G_i}, \tag{3}$$

$$\frac{1}{Q_V} = \frac{\int_{V_V} \varepsilon_V'' \varepsilon_0 |\mathbf{E}|^2 dV}{2W} = \eta_V \tan \delta_V, \tag{4}$$

where $\mathbf{E}$ is the electric field and $\mathbf{H}_\tau$ is the magnetic field tangential to the i-th metallic surface S_i with surface resistance R_i and geometrical factor G_i. η_S and η_V are the filling factors of the sample and of the dielectric elements inside the resonator, respectively. Thus:

$$\frac{1}{Q} = \eta_S \tan \delta_S + \sum_i \frac{R_i}{G_i} + \eta_V \tan \delta_V. \tag{5}$$

Since W and the field configuration depend on ε' of all the dielectric elements inside the resonator, both η and G are also functions of ε_S'. Therefore, to evaluate $\tan \delta_s$ of the dielectric sample placed in the resonator from Eq. (5), ε_S' must be measured. To achieve this aim, one can exploit f_0 of the resonator as a second measurand. However, it is known that the absolute value of f_0 is strongly affected by many intrinsic (e.g. the electromagnetic properties of the elements inside the resonator) and extrinsic (e.g. temperature, pressure, humidity) factors, meaning it is very difficult to utilise it in practice. However, the variation $\Delta f_0/f_{0,ref}$ of f_0, with respect to the reference value $f_{0,ref}$, is much more reliable due to the change of one or more parameters [15]. In this case, Δf_0, as caused by the insertion of the dielectric sample, is measured. Then, with electromagnetic simulations, Δf_0 is evaluated as a function of ε_S'. Thus, ε_S' is determined as the value at which the simulated Δf_0 coincides with the measured one. Thus, ε_S' is evaluated with the aid of e.m. simulations of the resonator.

After ε_S' is evaluated, the factors η and G in Eq. (5) can be analytically or numerically (with simulators) calculated. Following this, Eq. (5) can be inverted to obtain $\tan \delta_S$ from the Q measurements if all the R_i and $\tan \delta_V$ of the resonator are known from previous measurements or calibration procedures.

It must be mentioned that the unloaded Q in Eq. (5) differs in principle from the measured Q_l because of the coupling of the resonator with the external lines. However, with very small coupling (i.e. $P_{ext}/P < 0.01$, with P_{ext} being the losses in the external transmission lines), as in our set up, one has $Q_l \sim Q$ and $u(Q) \sim u(Q_l)$ [15].

The use of Eq. (5) can give unacceptably large uncertainties since, at microwave frequencies, the accuracy with which all the quantities in Eq. (5) are known is poor when compared to dc or low frequency measurements. In fact, in our case, $R = 92$ mΩ with $u(R)/R \sim 15\,\%$ and $\tan \delta_V = 4 \cdot 10^{-5}$ with $u(\tan \delta_V)/\tan \delta_V \sim 50\,\%$.

In order to reduce the effects of these uncertainties on $\tan \delta_s$, a perturbative approach is proposed here. The difference $\Delta(Q^{-1})$ between the measured quality factors Q_S^{-1} and Q_A^{-1}, obtained with the sample into the resonator (subscript S) or with a gap of air in its place (subscript A), respectively, can be written as:

$$\Delta(Q^{-1}) = \eta_S \tan \delta_S + \sum_i R_i \Delta(G_i^{-1}) + \Delta(\eta_V) \tan \delta_V, \tag{6}$$

where it is clear that the smaller $\Delta(G_i^{-1})$ and $\Delta(\eta_V)$ are, then the smaller their contributions to the uncertainties of R_i and $\tan \delta_V$ are.

2.1. Measurement system and procedure

The resonator used for this study is depicted in Figure 1. The single sapphire crystal is a cylinder (height $h = (5.0 \pm 0.1)$ mm,
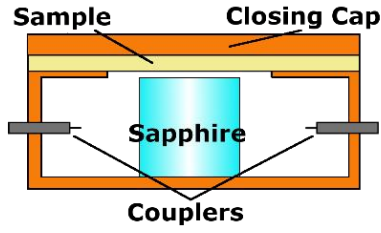
Figure 1. Sketch of the dielectric loaded resonator (not to scale).

diameter $\varnothing = (8.0 \pm 0.1)$ mm). A K-type coaxial transmission line, ending with coupling loops, is used to excite and sense (in transmission mode) the e.m. field configuration in the resonator. The dielectric samples are supported by a brass mask with a central hole $\varnothing = (13.00 \pm 0.01)$ mm and closed with a brass cap in order to prevent energy radiation, as depicted in Figure 1. The DR is excited in the TE_{011} mode, and thus, the $\boldsymbol{E}$ field is oriented parallel to the bases of the resonator. It is important to underline the orientation of the $\boldsymbol{E}$ field because the layered deposition techniques typical of most of the 3D-printers can generate anisotropic effects on the e.m. properties of the printed samples. A uniaxial anisotropy factor of almost 7 % was measured for ε' at 40 GHz for polylactide (PLA) samples using the waveguide reflection method [19]. In the method presented here, the $\boldsymbol{E}$ field is almost parallel to the deposition layers of the sample; thus, our results probe the direction along the layer deposition without significant mixing of the perpendicular component.

The resonator transmission complex scattering parameter S_{12}, from which Q and f_0 are evaluated, is measured with an Anritsu 37269D Vector Network Analyzer (VNA) in the following way:

- The VNA is calibrated using the Short Open Load Through (SOLT) method, and the 12-errors parameters are applied to the frequency range in which the measurements are performed;
- The transmission scattering parameter $S_{12}(f)$ is acquired with 1601 points evenly distributed in a frequency range width $7\Delta f_{-3dB}$, where Δf_{-3dB} is the width of the resonance curve at half power. Each data point is averaged with 10 acquisitions to reduce the noise contribution;
- The absolute value of the acquired points $|S_{12}(f)|$, which have the uncertainty $u(S_{21}(f))$, given by the VNA after the calibration [21], is fitted to the Fano resonance curve [22], [23]:

$$|S_{12}(f)| = \left| \frac{S_{12}(f_0)}{1 + 2iQ\frac{f - f_0}{f_0}} + S_c \right|, \tag{7}$$

where the complex constant S_c represents the cross-coupling contribution. For each resonance curve, Q and f_0 are evaluated with their uncertainties $u(Q)$, $u(f_0)$. The uncertainties of the fitted parameters are obtained by standard statistical methods starting with the fitting residuals variance σ_R^2 [24];

- For each mounting, 10 resonance curves are acquired. Then, the mean values of Q and f_0 are evaluated with their standard deviation: $u(Q)/Q \sim 0.05\%$ and $u(f_0)/f_0 \sim 1$ ppm;

- For each sample, 5 mountings are performed, disassembling and resetting the sample in its position. Then, the mean value of Q and f_0 with their standard deviation are evaluated. The final uncertainties $u(Q)/Q \sim 1\%$ and $u(f_0)/f_0 \sim 20$ ppm exist mainly due to the repeatability of the assembly.

3. UNCERTAINTIES ANALYSIS

In this section, the behaviour of the measurement technique is explored for the whole sample parameter space in order to establish the best working condition and its boundaries as a function of ε_s', $\tan\delta_s$ and sample thickness t.

First, the sensitivity of the resonator to $\tan\delta_s$ variations is analysed. The sensitivity is evaluated from Eq. (5) as:

$$c = \frac{\partial Q}{\partial \tan\delta_s} = -\frac{\eta_s}{(\eta_s \tan\delta_s + l_r)^2} = -\eta_s Q^2, \tag{8}$$

with $l_r = \sum_i \frac{R_i}{G_i} + \eta_V \tan\delta_V$, which, as a first approximation, in this analysis is assumed to be independent from the sample properties; in the small perturbation limit, the changes in the e.m. field configuration due to the sample are small and practically negligible, meaning the conduction/volume losses given by the resonator components do not change appreciably. In our case, $l_r \sim 5000 = Q_A^{-1}$.

In Figure 2, $|c(\tan\delta_s, \eta_s)|$ is reported for $10^{-5} < \tan\delta_s < 10^0$ and $\eta_s = \{10^{-4}, 10^{-3}, 10^{-2}, 10^{-1}\}$. One can notice a different $\log|c|$ slope m at high $\tan\delta_s$ values ($m = -2$) and at low $\tan\delta_s$ ($m = 0$) in the log–log plot (Figure 2). The $m = -2$ behaviour is due to the losses inside the dielectric samples when the following hold: $\eta_s \tan\delta_s \gg l_r$, and, from Eq. (8), $c \to -\eta_s^{-1}(\tan\delta_s)^{-2}$. Conversely, when $\eta_s \tan\delta_s \ll l_r$, $c \to -\eta_s l_r^{-2}$; as such, c is no longer dependent on $\tan\delta_s$. As expected, the bigger η_s, the higher $|c|$, as long as the sample losses are small. Thus, for low $\tan\delta_s$ samples, a higher η_s is preferable, while at higher $\tan\delta_s$, a lower η_s gives better performances.

At a fixed $\tan\delta_s$ value, the maximum sensitivity is obtained at the crossover of $|c|$ (see Figure 2); thus, $\eta_s = \eta_{s,opt} = l_r/\tan\delta_s$ and $|c|_{max} = (4l_r \tan\delta_s)^{-1}$. $\eta_{s,opt}$ is the optimum sample filling factor and gives the maximum sensitivity for Q measurements. As such, the geometry of the samples under
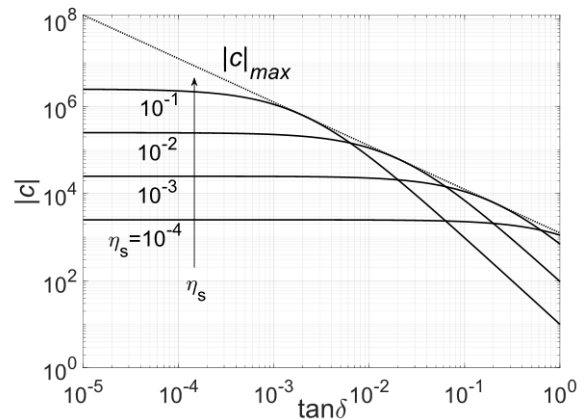
Figure 2. Solid lines: the absolute value of resonator sensitivity $|c|$ as a function of the sample $tan\delta_s$ and filling factor η_s. Dotted line: the maximum sensitivity $|c|_{max}$ reachable for every $tan\delta_s$ value.

investigation can be adjusted in order to fulfil the requirement for $\eta_{s,opt}$. In our case, this is the expected $\tan \delta_s \sim 10^{-2}$. So, from Figure 2, $\eta_{s,opt} \sim 10^{-2}$.

The loss tangent measurement uncertainty $u(\tan \delta_s)$ is evaluated as follows [20]:

$$
\begin{aligned}
u^2(\tan \delta_S) \\
= \frac{1}{\eta_S^2}\Bigg[&\left(u\left(\Delta(Q^{-1})\right)\right)^2 + \sum_i \left(\Delta(G^{-1})u(R_i)\right)^2 \\
&+ \sum_i \left(R_i u\left(\Delta(G^{-1})\right)\right)^2 + \left(\tan \delta_V u\left(\Delta(\eta_V)\right)\right)^2 \\
&+ \left(\Delta(\eta_V)u(\tan \delta_V)\right)^2 + \left(\tan \delta_S u(\eta_S)\right)^2 \Bigg],
\end{aligned}
\tag{9}
$$

with:

$$
u^2\left(\Delta(Q^{-1})\right) = \left(\frac{u(Q_S)}{Q_S^2}\right)^2 + \left(\frac{u(Q_A)}{Q_A^2}\right)^2,
\tag{10}
$$

$$
\begin{aligned}
u^2\left(\Delta(G^{-1})\right) &= \left(\frac{u(G_{i,S})}{G_{i,S}^2}\right)^2 + \left(\frac{u(G_{i,A})}{G_{i,A}^2}\right)^2 \\
&- 2r_G \frac{u(G_{i,S})u(G_{i,A})}{G_{i,S}^2 G_{i,A}^2},
\end{aligned}
\tag{11}
$$

$$
u^2\left(\Delta(\eta_V)\right) = u^2(\eta_{V,S}) + u^2(\eta_{V,A}) - 2r_\eta u(\eta_{V,S})u(\eta_{V,A}).
\tag{12}
$$
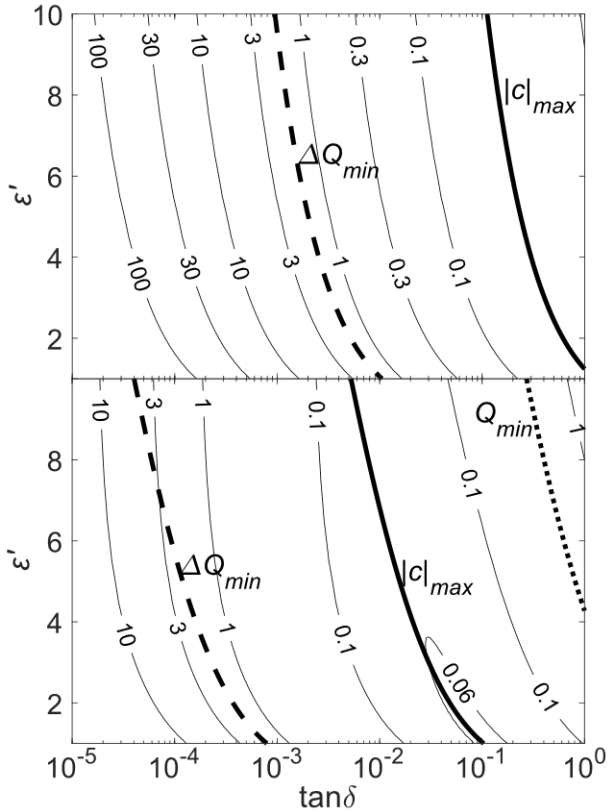
Figure 3. Relative loss tangent uncertainty $u(tan \delta_S)/tan \delta_S$ contour plot in the plane $(\varepsilon', \tan \delta)$ for samples of thickness $t = 0.5$ mm (upper panel) and $t = 1.5$ mm (lower panel). The thicker solid line represents the points of maximum sensitivity $|c|_{max}$ as evaluated from Figure 2. The dashed line corresponds to the minimum quality factor appreciable variation $\Delta Q_{min} = Q_A - Q_S \sim 40$ and the dotted line to the minimum evaluable $Q_{S,min} \sim 100$.

The correlation factors r_G and r_η are supposed to be almost 1 since the evaluation of G_i and η_V is performed with the same algorithm and with the same settings. Conversely, the Q measurements are not strongly correlated, since the different mountings can introduce different uncorrelated error contributions.

Next, $u(\tan \delta_s)$ is explored in the space $(1 < \varepsilon' < 10, 10^{-5} < \tan \delta_s < 10^0, 0.5 \text{ mm} < t < 2 \text{ mm})$ to establish the operative limits of this technique. $u(\tan \delta_s)$ is evaluated using Eq. (9) with geometrical G factors and filling η factors obtained through e.m. simulations. Using e.m. simulations, it has been verified that $\tan \delta_s$ variations (in the studied space) do not alter the e.m. field configuration. Therefore, for the evaluation of G and η, $\tan \delta_s$ is fixed (i.e. $\tan \delta_s = 10^{-2}$). Both $u(G)$ and $u(\eta)$ are obtained with Monte Carlo e.m. simulations randomly varying all the physical dimensions and the e.m. properties of the materials from which the resonator is made in their uncertainty space [25].

It should be noted that $u(Q)/Q$ is ideally constant for every Q value if the measurement frequency span is kept proportional to f_0/Q and the number of points constant [26]. Yet, because of the mounting repeatability limitation, the presence of other resonance modes and other unideal factors (e.g. a complex background signal on the transmission parameter and a cross-coupling contribution), $u(Q)$ is somehow limited even at low Q. As such, its absolute value is assumed constant, i.e. $u(Q) \sim 40$. In Figure 3, $u(\tan \delta_s)/\tan \delta_s$ is evaluated in the plane $(\varepsilon', \tan \delta)$, and it is reported for samples with $t = 1.5$ mm and $t = 0.5$ mm. $u(\tan \delta_s)/\tan \delta_s$ strongly depends on the sample thickness t and, thus, on η_s, as expected from Figure 2. $u(\tan \delta_s)$ sharply increases with thinner samples, particularly at low $\tan \delta_s$ values: with $\tan \delta_s \sim 10^{-2}$ and $\varepsilon_s' \sim 2$, $u(\tan \delta_s)/\tan \delta_s \sim 100 \%$ for a 0.5 mm thick sample, while $u(\tan \delta_s)/\tan \delta_s \sim 10 \%$ in the same conditions but $t = 1.5$ mm. In Figure 3, the $\varepsilon_s'(\tan \delta_s)$ curve corresponding to $|c|_{max}$ is reported; it agrees to a fair extent with the lowest $u(\tan \delta_s)/\tan \delta_s$ level.

Once the maximum $u(\tan \delta_s)$ threshold level is fixed, taking what is shown in Figure 3, the space $(\varepsilon', \tan \delta)$ where the proposed technique can be reliably used is defined. However, two other limiting factors must be considered. The first is related to the impossibility to discriminate small $\Delta Q \sim Q_A - Q_S$ variations because of the measurement noise. Thus, where $\Delta Q < \Delta Q_{min}$, this technique is no more sensitive. In our case, with $Q_A \sim 5000$, $\Delta Q_{min} \sim 40$. In Figure 3, the ΔQ_{min} curve is reported; however, one can notice that it crosses the $(\varepsilon', \tan \delta)$ plane where $u(\tan \delta_s)/\tan \delta_s > 100 \%$. The second limit is set where the losses of the sample are so high as to make Q_S too small to be reliably measured. Due to the $S_{12}(f)$ background, we set this minimum value $\min(Q_s) \sim 100$. In Figure 3, the dotted line represents this limit: above this curve no $\tan \delta_s$ measurements are possible.

The presented technique can be easily optimized for the characterization of these materials. In fact, the position of the minimum of $u(\tan \delta_s)/\tan \delta_s$ shown in Figure 3 arises in the region of the expected values of ε_s' and $\tan \delta_s$ of 3D-printer materials, and it can be tuned with η_s.

Table 1. The mean thickness $\bar{t}$ of the samples and its standard deviation σ_t.

	S_1	S_2	S_3	S_4
$\bar{t}$ (mm)	0.522	1.002	1.512	2.063
σ_t (mm)	0.003	0.004	0.005	0.004

Table 2. The inverse of the measured quality factors when the four samples, $S1$-$S4$, are inserted. Q_S^{-1} and Q_A^{-1} refer to the measurement with the sample or an air gap of equal thickness, respectively.

	S_1	S_2	S_3	S_4
$Q_S^{-1} \cdot 10^4$	2.15	2.48	3.06	4.25
$Q_A^{-1} \cdot 10^4$	1.95	1.96	1.98	2.00

4. RESULTS AND DISCUSSION

The measurements were performed on four dielectric samples, which were of different thickness values t as reported in Table 1, made of a photopolymer material printed using the PolyJet™ deposition technique. The thicknesses and flatnesses of the samples were checked with a micrometre. The mean values $\bar{t}$ and their standard deviation $\sigma_t = \sqrt{\sum_{i=1}^{N}(t - \bar{t})^2/(N-1)}$ have been obtained by $N = 10$ different measurements of the thickness by probing the surfaces of the samples. Thus, σ_t can be read as a measure of the flatness of the samples.

To achieve a sufficiently sensitive method of evaluating ε', the frequency repeatability of the setup needs to be reliable to allow the accurate measurement of the differences between $f_{0,S}$ (measured with the dielectric samples mounted) and $f_{0,A}$ (measured without the sample and leaving an air gap of the same sample thickness). This is achieved using 3D-printed rings prepared in the same way and of the same thickness as the dielectric samples. The data are presented in Figure 4, from which one can then evaluate $\varepsilon'_S = 2.9 \pm 0.2$.

Once ε'_S is estimated with its uncertainty, the geometrical and filling factors of the resonator components (with their uncertainties) are evaluated from the simulations as shown in the previous section.

Then, $\tan \delta_S$ is evaluated through Eq. (6) from the measured $\Delta(Q^{-1}) = Q_S^{-1} - Q_A^{-1}$. The quality factors Q are reported in Table 2.

In Figure 5, the measured $\tan \delta_S$ is shown with the error bars evaluated with Eq. (9) using the uncertainties for the measured quantities and simulated parameter shown previously. Figure 5 shows the best estimate: $\tan \delta_S = (1.8 \pm 0.2) \cdot 10^{-2}$ as calculated with $\varepsilon'_S = 2.9 \pm 0.2$. The evaluation of $\tan \delta_S$ is performed taking as best value the centre point in the common confidence interval of all the experimental points (the light blue

band in Figure 5). Then, the uncertainty is the half width of that common interval. One can note that the uncertainty bars rapidly increase in size when the sample thickness becomes small due to a lack of sensitivity, as expected from the analysis presented in Sec. 3. This effect is present also in Figure 4, where the simulated curves for small thickness values tend to coalesce. Conversely, samples with a large thickness can cause e.m. field radiation from the structure, thereby significantly changing the resonant mode and adding further losses. The method presented here, in our geometry, is then most suitable for samples of thickness between 1 and 2 mm.

5. CONCLUSIONS

In this work, a dielectric loaded-resonator-based technique was developed and presented for the measurement of the complex permittivity $\tilde{\varepsilon}$ of 3D-printing materials. We exploited the possibility of shaping the sample into appropriate shapes (disks, in our case) and the excellent frequency repeatability of our setup to reliably measure the quality factor Q and the resonance frequency f_0 both with and without the sample loaded into the cavity. From the variations of Q and f_0 given by the sample insertion, $\tilde{\varepsilon}$ is obtained using the perturbation approach. The measurement technique performances were deeply analysed in terms of sensitivity and accuracy in the whole parameter space in order to establish the sample geometry, as a function of its e.m. properties, for the best measurement accuracy.

The technique was tested by measuring photopolymer material printed using PolyJet™ deposition. With the presented technique here, it was obtained that $\varepsilon'_S = 2.9 \pm 0.2$ and $\tan \delta_S = 0.018 \pm 0.002$.

The obtained result agrees well with other studies. In particular, using a combined technique, a broad band (1 MHz÷11 GHz) characterisation of 3D-printer materials was presented in [13]. The high frequency range (8.2 GHz÷11 GHz)

Figure 4. Differences between the resonant frequencies $f_{0,S}$ (with the samples mounted) and $f_{0,A}$ (with the sample substituted by an air gap of the same thickness). The red dots are the experimental data and the blue lines the simulations results.
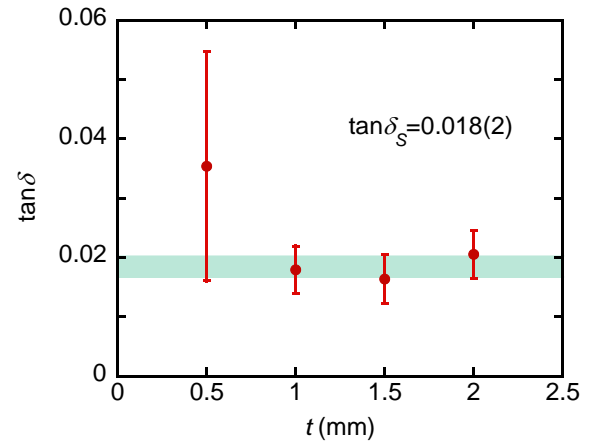
Figure 5. The measured loss tangent of the dielectric 3D-printed material $\tan \delta_S$. The error bars are evaluated with Eq. (9) and the green area represents the confidence interval.
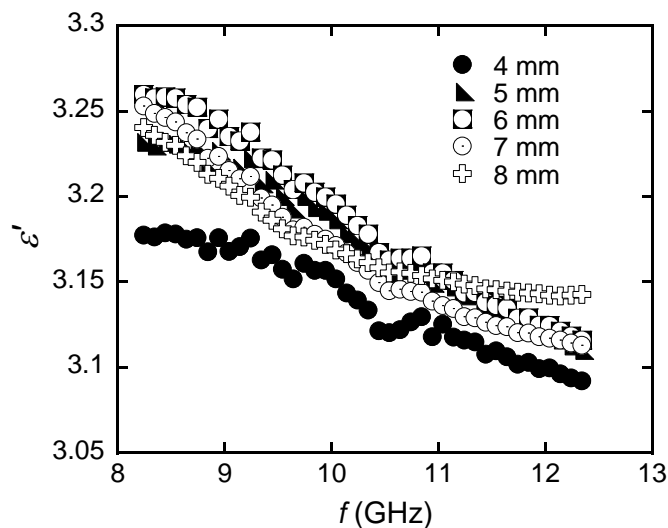
Figure 6. Real part of the complex permittivity $\Re\{\tilde{\varepsilon}\} = \varepsilon'$ measured on dielectric samples of different thicknesses using the 'NIST precision' transmission/reflection method [26] through a WR90 waveguide.

was studied through a waveguide in reflection mode, although an uncertainty study was lacking in this frequency range. The reported values at 11 GHz were $2.5 < \varepsilon' < 3.29$ and $0.005 < \tan \delta < 0.037$, perfectly in agreement with our results.

In order to check the accuracy of the DR technique shown in this paper, $\tilde{\varepsilon}$ of the studied materials was also measured with a standard reflection/transmission method. A WR90 waveguide was used with a PNA Network Analyzer (model E8363C, Agilent Technologies) with the Agilent 85071E software and the 'NIST precision' method [27]. To perform this measurement, parallelepipeds of $22.8 \cdot 10.1$ mm² and different thicknesses (4, 5, 6, 7, 8 mm) were printed. $\varepsilon_S' \sim 3.1$ was measured by extrapolating the value at 12.9 GHz, and no significative sample variations can be seen (Figure 6). This value compares well with the one obtained using the proposed DR technique and the f_0 variation.

Then, the imaginary part $\varepsilon_S'' \sim 0.23$ is obtained with the waveguide method, which yields $\tan \delta_s \sim 0.074$ with a significant inter-sample scattering. This value is about 4 times higher than the one obtained with the DR method. However, it must be mentioned that the 'NIST precision' method was developed to solve the accuracy problems of the Nicholson–Ross–Weir technique (NRW) near the sample resonances [15], [27]. The 'NIST precision' and the NRW give comparable results out of the resonances. It is well known that the NRW is not a reliable method for the ε'' evaluation of low-loss materials. In fact, the same measurement fixture was tested with a Polytetrafluoroethylene sample obtaining $\varepsilon_{PTFE}'' \sim 1.5 \times 10^{-2}$. However, from the literature [28], this is expected to be about two orders of magnitude smaller. Also, for materials with higher losses, NRW accuracy is limited; the comparison presented in [29] between the NRW and other methods shows some discrepancies, even at $\tan \delta \sim 10^{-2}$ values (e.g. with nylon samples), as in our case. Thus, the disagreement between the DR $\tan \delta$ measurement and that obtained in waveguide, which was somewhat expected, will be studied in further works.

In summary, a new measurement technique was presented for the e.m. characterisation of dielectric materials, with interesting potential applicability to industrial fields due to its simple conceptual approach and high accuracy.

REFERENCES

[1] N. Hopkinson, P. Dickens, Emerging rapid manufacturing processes, in: Rapid Manufacturing; an Industrial Revolution for the Digital Age. N. Hopkinson, R. Hague, P. Dickens (editors). Wiley & Sons Ltd, Chichester, 2006, ISBN: 0-470-01613-2, pp. 55-80.

[2] M. J. Werkheiser, J. Dunn, M. P. Snyder, J. Edmunson, K. Cooper, M. M. Johnston, 3D printing in zero-g ISS technology demonstration, AIAA SPACE 2014 Conference and Exposition, San Diego, California, 2014, pp 2054-2078.

[3] J. Y. Wong, Ultra-portable solar-powered 3D printers for onsite manufacturing of medical resources, Aerospace Medicine and Human Performance 89 (2015) pp. 830-834.
DOI: https://doi.org/10.3357/AMHP.4308.2015

[4] C. Schubert, M. C. Van Langeveld, L. A. Donoso, Innovations in 3D printing: a 3D overview from optics to organs, British Journal of Ophthalmology 98 (2014) pp. 159-161.
DOI: https://doi.org/10.1136/bjophthalmol-2013-304446

[5] F. Rengier, A. Mehndiratta, H. Von Tengg-Kobligk, C. M. Zechmann, R. Unterhinninghofen, H. Kauczor, F. L. Giesel, 3D printing based on imaging data: review of medical applications, International Journal of Computer Assisted Radiology and Surgery 5 (2010) pp. 335-341.
DOI: https://doi.org/10.1007/s11548-010-0476-x

[6] M. J. Burfeindt, T. J. Colgan, R. O. Mays, J. D. Shea, N. Behdad, B. D. Van Veen, S. C. Hagness, MRI-derived 3-D-printed breast phantom for microwave breast imaging validation, IEEE Antennas and Wireless Propagation Letters 11 (2012) pp. 1610-1613.
DOI: https://doi.org/10.1109/LAWP.2012.2236293

[7] A. T. Mobashsher, A. M. Abbosh, Three-dimensional human head phantom with realistic electrical properties and anatomy, IEEE Antennas and Wireless Propagation Letters 13 (2014) pp. 1401-1404.
DOI: https://doi.org/10.1109/LAWP.2014.2340409

[8] A. Bisognin, A. Cihangir, C. Luxey, G. Jacquemod, R. Pilard, F. Gianesello, W. G. Whittow, Ball grid array-module with integrated shaped lens for WiGig applications in eyewear devices, IEEE Transactions on Antennas and Propagation 64 (2016) pp. 872-882.
DOI: https://doi.org/10.1109/TAP.2016.2517667

[9] G. P. Le Sage, 3D printed waveguide slot array antennas, IEEE Access 4 (2016) pp. 1258-1265.
DOI: https://doi.org/10.1109/ACCESS.2016.2544278

[10] A. Rashidian, L. Shafai, M. Sobocinski, J. Peräntie, J. Juuti, H. Jantunen, Printable planar dielectric antennas, IEEE Transactions on Antennas and Propagation 64 (2016) pp. 403-413.
DOI: https://doi.org/10.1109/TAP.2015.2502265

[11] P. Nayeri, M Liang, R. A. Sabory-Garcı, M. Tuo, F. Yang, M. Gehm, A. Z. Elsherbeni, 3D printed dielectric reflectarrays: low-cost high-gain antennas at sub-millimeter waves, IEEE Transactions on Antennas and Propagation 62 (2014) pp. 2000-2008.
DOI: https://doi.org/10.1109/TAP.2014.2303195

[12] C. R. Garcia, R. C. Rumpf, H. H. Tsang, J. H. Barton, Effects of extreme surface roughness on 3D printed horn antenna, Electronics Letters 49 (2013) pp. 734-736.
DOI: https://doi.org/10.1049/el.2013.1528

[13] P. I. Deffenbaugh, R. C. Rumpf, K. H. Church, Broadband microwave frequency characterisation of 3-D printed materials, IEEE Transactions on Components, Packaging and Manufacturing Technology 3 (2013) pp. 2147-2155.
DOI: https://doi.org/10.1109/TCPMT.2013.2273306

[14] T. D. Ngo, A. Kashani, G. Imbalzano, K. T. Nguyen, D. Hui, Additive manufacturing (3D printing): A review of materials, methods, applications and challenges, Composites Part B: Engineering 143 (2018) pp. 172-196.
DOI: https://doi.org/10.1016/j.compositesb.2018.02.012

[15] L. F. Chen, C. K. Ong, C. P. Neo, V. V. Varadan, V. K. Varadan, Microwave Electronics: Measurement and Materials Characterisation., John Wiley & Sons, Chichester, 2004, ISBN: 0-470-84492-2.

[16] J. Mazierska, C. Wilker, Accuracy issues in surface resistance measurements of high temperature superconductors using dielectric resonators (corrected), IEEE Transactions on Applied Superconductivity 11 (2001) pp. 4140-4147.
DOI: https://doi.org/10.1109/77.979858

[17] J. Mazierska, M. V. Jacob, How accurately can the surface resistance of various superconducting films be measured with the sapphire Hakki–Coleman dielectric resonator technique?, Journal of Superconductivity and Novel Magnetism 19 (2006) pp. 649-655.
DOI: https://doi.org/10.1007/s10948-006-0129-z

[18] F. Castles, D. Isakov, A. Lui, Q. Lei, C. E. J. Dancer, Y. Wang, J. M. Janurudin, S. C. Speller, C. R. M. Grovenor, P. S. Grant, Microwave dielectric characterisation of 3D-printed BaTiO3/ABS polymer composites, Scientific Reports 6 (2016) art. no. 22714
DOI: https://doi.org/10.1038/srep22714

[19] J. M. Felício, C. A. Fernandes, J. R. Costa, Complex permittivity and anisotropy measurement of 3D-printed PLA at microwaves and millimeter-waves, 22nd International Conference on Applied Electromagnetics and Communications (ICECOM), Dubrovnik, Croatia, 2016, pp. 54-60.

[20] B. W. Hakki, P. D. Coleman, A dielectric resonator method of measuring inductive capacities in the millimeter range, IRE Transactions on Microwave Theory and Techniques 8 (1960) pp. 402-410.
DOI: https://doi.org/10.1109/TMTT.1960.1124749

[21] K. Torokhtii, A. Alimenti, N. Pompeo, F. Leccese, F. Orsini, A. Scorza, S. A. Sciuto, E. Silva, Q-factor of microwave resonators: calibrated vs. uncalibrated measurements, Journal of Physics: Conference Series 1065 (2018) art. no. 052027.
DOI: https://doi.org/10.1088/1742-6596/1065/5/052027

[22] K. Leong, J. Mazierska, Precise measurements of the Q factor of dielectric resonators in the transmission mode-accounting for noise, crosstalk, delay of uncalibrated lines, coupling loss, and coupling reactance, IEEE Transactions on Microwave Theory and Techniques 50 (2002) pp. 2115-2127.
DOI: https://doi.org/10.1109/TMTT.2002.802324

[23] N. Pompeo, K. Torokhtii, F. Leccese, A. Scorza, A. S. Sciuto, E. Silva, Fitting strategy of resonance curves from microwave resonators with non-idealities, IEEE International Instrumentation and Measurement Technology Conference (I2MTC), Torino, Italy, 2017, pp. 1-6.
DOI: https://doi.org/10.1109/I2MTC.2017.7969903

[24] ISO/IEC GUIDE 98-3:2008 - Guide to the expression of uncertainty in measurement (GUM:1995).

[25] ISO/IEC GUIDE 98-3/Suppl.1:2008 - Propagation of distributions using a Monte Carlo method.

[26] K. Torokhtii, A. Alimenti, N. Pompeo, E. Silva, Uncertainty in uncalibrated microwave resonant measurements, Proc. of the 23rd IMEKO TC4 International Symposium Electrical & Electronic Measurements Promote Industry 4.0, Xi'An, China, 2019, pp. 98-101. Online [Accessed 24 September 2020]
https://www.imeko.org/publications/tc4-2019/IMEKO-TC4-2019-022.pdf

[27] J. Baker-Jarvis, E. J. Vanzura, W. A. Kissick, Improved technique for determining complex permittivity with the transmission/reflection method, IEEE Transactions on microwave theory and techniques 38 (1990) pp. 1096-1103.
DOI: https://doi.org/10.1109/22.57336

[28] J. Krupka, Measurements of the complex permittivity of low loss polymers at frequency range from 5 GHz to 50 GHz, IEEE Microwave and Wireless Components Letters 26 (2016) pp. 464-466.
DOI: https://doi.org/10.1109/LMWC.2016.2562640

[29] Z. Abbas, R. D. Pollard, R. W. Kelsall, Complex permittivity measurements at Ka-band using rectangular dielectric waveguide, IEEE Transactions on Instrumentation and Measurement 50, (2001) pp. 1334-1342.
DOI: https://doi.org/10.1109/19.963207